Received: 11 October 2017 | Revised: 31 March 2018 | Accepted: 19 May 2018 | Published on: 5 August 2018

DOI: 10.1002/joc.5726

International Journal of Climatology RMetS

SHORT COMMUNICATION

Upscaling impact of wind/sea surface temperature mesoscale interactions on southern Africa austral summer climate

Fabien Desbiolles[1] | Ross Blamey[1] | Serena Illig[1,2] | Rachel James[1,3] | Rondrotiana Barimalala[1] | Lionel Renault[2,4] | Chris Reason[1]

[1]Department of Oceanography, University of Cape Town, Cape Town, South Africa

[2]Laboratoire d'Etudes en Géophysique et Océanographie Spatiale (LEGOS), ICEMASA/CNRS/IRD/UPS/CNES, Toulouse, France

[3]School of Geography and the Environment, University of Oxford, Oxford, UK

[4]Department of Atmospheric and Oceanic Sciences, University of California, California, Los Angeles

Correspondence
Fabien Desbiolles, Department of Oceanography, University of Cape Town, Cape Town, South Africa.
Email: fabien.desbiolles@uct.ac.za

Funding information
Natural Environment Research Council; NERC

Mesoscale sea surface temperature (SST) variability plays an important role in shaping local atmospheric boundary layers through thermodynamic processes. This study focuses on the upscaling effects of mesoscale SST gradients in sensitive areas on the southern Africa regional atmospheric circulation. Using regional atmospheric model sensitivity experiments which differ only in the mesoscale SST forcing characteristics (either the full spectrum of SST variability or only its large-scale components are included), we first quantify the importance of SST gradients on regional atmospheric conditions. Agulhas eddies and meanders influence the vertical air column up to the troposphere, and mesoscale ocean patterns significantly modify incoming landwards moisture fluxes. The austral summer mean state is then modified in terms of air temperature, cloud cover and mean rainfall, with notable differences in tropical rainbands over southwestern Africa. Mesoscale SST variability favours tropical–extra-tropical interactions and cloudband development over the continent. These results stress the importance of high-resolution ocean forcing for accurate atmospheric simulations.

KEYWORDS

atmospheric circulation, mesoscale SST forcing, rainfall variability, southern Africa summer climate, upscaling effects of mesoscale air–sea interactions

1 | INTRODUCTION

Many interactions and coupling processes coexist over a large spectrum of temporal and spatial scales at the air–sea interface. Both one- and two-way interactions between the ocean and atmosphere are key features in driving circulation in both fluids and are therefore paramount for determining the roles of the ocean and atmosphere in climate variability (Chelton and Xie, 2010).

It has been commonly assumed that the large-scale upper ocean dynamics is driven by wind energy inputs as well as radiative and turbulent heat fluxes (Gill, 1982). However, on smaller spatial and temporal scales, the ocean imprints on to the atmosphere, notably through thermodynamic and dynamic processes (Chang and Philander, 1994). These processes strongly influence the marine atmospheric boundary layer (MABL), with ocean feedbacks on the atmosphere

Abbreviations: ABFZ, Angola–Benguela frontal zone, BUS, Benguela upwelling system, CFSR, NCEP Climate Forecast System Reanalysis, DJF, austral summer months: December–January–February, ERA-Interim, European Reanalysis developed at ECMWF, ECMWF, European Centre for Medium-Range Weather Forecasts, ITCZ, Intertropical Convergence Zone, MABL, marine atmospheric boundary layer, MUR SST, multi-scale ultra-high resolution sea surface temperature, NCEP, National Centers for Environmental Prediction, NCEP-FNL, NCEP Final Reanalysis, OSTIA, Operational Sea Surface Temperature and Sea Ice Analysis, PBL, planetary boundary layer, SST, sea surface temperature, TOA, top-of-atmosphere, WRF, Weather Research and Forecasting model

having been clearly identified at the ocean mesoscale, especially over strong mid-latitude sea surface temperature (SST) fronts generated by meandering ocean currents (Small *et al*., 2008; O'Neill *et al*., 2010). The thermodynamics feedback entails an air parcel warming over the warm flank of the front or a mesoscale structure (i.e., eddy), involving the destabilization of the MABL, and thus the intensification of both vertical turbulent mixing and convection (Song *et al*., 2009). Furthermore, the mitigation (development) of the vertical shear profile within the planetary boundary layer (PBL) contains strong near-surface signatures (i.e., the acceleration (deceleration) of the wind over warm (cold) waters). This SST/wind interaction satisfies a roughly linear relationship between the two fields, which has already been quantified over coherent mesoscale structures (e.g., Chelton *et al*., 2004; Small *et al*., 2008; O'Neill *et al*., 2010; Desbiolles *et al*., 2014). Minobe *et al*. (2008) have shown that over the Gulf Stream meander structures, air–sea interactions at mesoscales can also affect the free atmosphere above the MABL on monthly and even longer timescales.

In this paper, we examine the influence of mesoscale SST patterns on the overlying atmosphere at a seasonal timescale, based on model experimentation with a regional Weather Research and Forecasting model (WRF) configuration. Often, coarse resolution SST products derived from reanalysis (such as CSFR (Saha *et al*., 2014) or ERA-Interim (Dee et al., 2011)) are prescribed as ocean surface boundary conditions for atmospheric simulations. However, Song *et al*. (2009) stressed the importance of mesoscale patterns in the SST forcing. They highlighted the increased fine-scale wind variability in ECMWF outputs associated with changes in SST resolution. Fine-scale modifications of the wind play a major role in shaping atmospheric processes, such as wind convergence (divergence) leading to convection (subsidence), cloud formation, moisture transport and rainfall variability. Further investigation linking the wind circulation and the mesoscale activity of the SST is therefore crucial.

The southern African region represents an ideal laboratory to quantify the role of air–sea interactions at mesoscale in shaping atmospheric patterns and properties at regional and seasonal timescales. Indeed, the oceans surrounding southern Africa are characterized by intense mesoscale activity (i.e., ocean features of order 10–100 km in horizontal scale), associated with the warm Agulhas Current, its meanders and eddies, the Benguela upwelling system (BUS), with its cold upwelling filaments, and the Angola–Benguela frontal zone (ABFZ). Thus, in the context of this study, oceanic mesoscale features refer to both eddies and to frontal SST gradients such as in the ABFZ or across the edge of the Agulhas Current. Although the large-scale influence of the ocean on southern African precipitation and general climate is fairly well documented (e.g., Mason, 1995; Reason and Mulenga, 1999; Behera and Yamagata, 2001; Reason *et al*., 2006), the influence of mesoscale SST gradients are poorly understood. It is yet unknown whether they impact the southern African climate through upscaling effects, that is, at a larger time and spatial scale than the one for which the process holds (about 100–1,000 km, weekly to monthly; e.g., Chelton *et al*., 2004; Desbiolles *et al*., 2014; 2017). Thus, the present study aims to address the upscaling effects of mesoscale SST gradients on the regional atmospheric circulation over the southern African region. Using a set of WRF numerical experiments which differ in mesoscale SST forcing characteristics, we first quantify local surface wind modifications due to mesoscale SSTs (section 2). Section 3 assesses the influence on the whole vertical air column, with a particular focus on the atmospheric responses above the MABL over Agulhas meanders, and the implications for incoming landward moisture fluxes over the subcontinent. Section 4 quantifies the integrated role of mesoscale dynamics on the seasonal mean state of southern Africa's climate. Finally, the conclusions are presented in section 5.

2 | MODEL EXPERIMENTS AND SURFACE RESPONSES TO SST MODIFICATIONS

The sensitivity of local and regional atmospheric features to mesoscale SST is investigated with the advanced research WRF model (Skamarock *et al*., 2005). The domain covers the southern African region with an 18 km horizontal resolution, extending from 45°–5°S and 5°W–65°E (see Figure 1a, b for the domain). To adequately represent MABL processes, 51 vertical levels are used, with half of them sampling the lowest 2 km (which roughly corresponds to the MABL over the open ocean). The model is initialized with the NCEP Final Reanalysis (NCEP-FNL, ~1° spatial resolution) from August 1, 2008, and first integrated for a month and 2 days to allow for the spin-up and to define a set of initial conditions (see below) for the subsequent experiments. Then, various experiments are conducted for the period September 2008 to May 2009, using 6-hourly lateral boundary conditions from NCEP-FNL. This period was chosen because summer 2008–2009 was a neutral El Niño–Southern Oscillation (ENSO) season, and ENSO has been documented to be one of the key drivers of inter-annual variability over southern Africa (Lindesay, 1988; Reason *et al*., 2000).

In order to study the effects of SST gradients on the regional atmospheric circulation, two sets of sensitivity experiments were carried out, using the same grid and physical parameterizations (detailed in Renault *et al*., 2016a; 2016b). The experiments only differ in the prescribed SST boundary conditions. The *Ctrl* runs are forced by the full spatial spectrum SST maps, built from the ~5 km resolution OSTIA daily product (Stark *et al*., 2007). The *noMeso-SST* experiments are forced with only the large-scale components of SST variability included and are calculated by applying a low-pass Lanczos filter to the original SST, with 2D-half-power filter cut-off wavelengths of 10° (~1,000 km, in

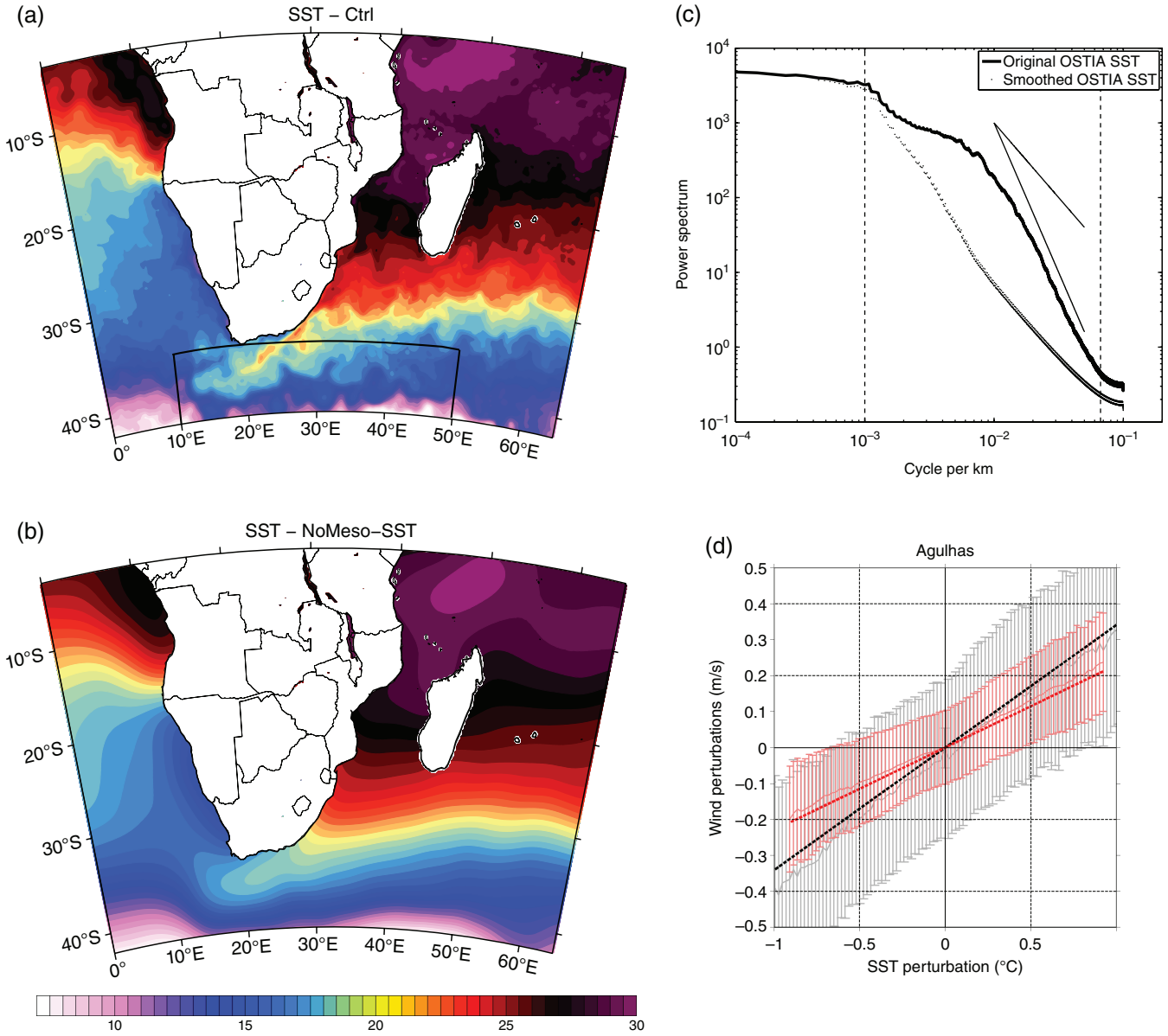

FIGURE 1 Snapshot of SST (°C) on December 4, 2008 for the *Ctrl* (a) and *noMeso-SST* (b) forcing fields. (c) One-month (January 2009) average of daily wave number spectra ($°C^2$) of ~5 km resolution original (bold line) and smoothed (dashed line) OSTIA SST computed over the WRF domain (a). For comparison, theoretical profiles in k^{-2} and k^{-4} are drawn (thin lines). (d) Binned scatterplot of 10 m wind speed perturbations (m/s) versus OSTIA SST perturbations (°C) for observed QuikSCAT and *Ctrl* run outputs in grey and red, respectively. Analysis is performed over DJF months using 15-day SST and wind speed running averages over the Agulhas region (black frame in (a). Each bin represents a 1/200 of the central 95% of the distribution. The bars indicate plus and minus one standard deviation about the average drawn with bold line. Spatial perturbations are isolated from large-scale features using a Lanczos filter with 2D-half-power filter cut-off wavelengths of 10° [Colour figure can be viewed at wileyonlinelibrary.com]

latitude and longitude). In each experiment set, an ensemble of five runs integrated with different initial conditions is obtained and the ensemble mean of each set is analysed and referred to as, *Ctrl* and *no-MesoSST*. The different initial conditions used for the ensemble correspond to the 00h00 WRF *Ctrl* atmospheric conditions for the August 30, 2008; August 31, 2008; September 1, 2008; September 2, 2008; and March 9, 2008 for the *Ctrl* and *NoMeso-SST* experiments that are then integrated from September 1, 2008 to May 31, 2009 in each case. Figure 1a,b presents an example of SST snapshots for both surface boundary fields, interpolated onto the WRF grid. The spatial variance of the SST is drastically impacted by our smoothing procedure. For instance, over the Agulhas region (black box in Figure 1a), the average spatial variance in SST during austral summer is 0.26 $°C^2$ for *Ctrl*, and 0.06 $°C^2$ for *noMeso-SST*. To illustrate the differences in the spatial scales resolved, Figure 1c shows 1-month averages of daily wave number spectra, computed with the original and smoothed SST fields. As expected, results show that spatial scales shorter than 1,000 km, which roughly correspond to the upper bounds of mesoscale processes, are smoothed in the *noMeso-SST* forcing field. A transfer function analysis shows that the −3 dB is reached at about 650 km (not shown). This analysis also

allows quantification of the effective resolution of OSTIA SST (e.g., Milliff *et al*., 2004; Lefèvre *et al*., 2010; Desbiolles *et al*., 2017). The OSTIA SST spectrum portrays a sharp change at ~20–25 km (dashed line in Figure 1c). This abrupt modification corresponds to its related effective resolution, which is approximately four grid points of the original OSTIA grid. Hence, the effective resolution of the OSTIA SST daily fields is suitable for the 18-km WRF simulations performed in this study.

In order to take into account the diurnal variation of the SST, the diurnal cycle is estimated from 6-hourly NCEP-FNL SST, as the departure from the daily mean SST at each model grid point. The latter is then added to both *Ctrl* and *noMeso-SST* forcing fields.

Figure 1d shows a binned scatterplot of 15-day running averages of the SST and 10 m wind speed perturbation fields over the Agulhas region (black box in Figure 1a) during the austral summer months (December–January–February [DJF] hereafter), for the WRF *Ctrl* run (in red) and for observed 0.25 × 0.25° QuikSCAT data (in grey). Spatial perturbations are defined as the high-pass filtered fields (for both wind speed—*Ctrl* run and QuikSCAT and SST–OSTIA), using a 2D-half-power Lanczos filter (with a cut-off wavelength defined at 10°). This classic diagnostic (e.g., Chelton *et al*., 2004; 2007; Desbiolles *et al*., 2014; 2017) highlights a strong correspondence between SST and wind perturbations, following a roughly linear relationship in *Ctrl*, while no linear relationship or significant correlation between SST and surface winds are found for the *noMeso-SST* runs (not shown). This result confirms that wind speed variability is locally driven by SST perturbations in the *Ctrl* run, consistent with the observations (Desbiolles *et al*., 2017). We however note a slight underestimation of the coupling coefficient in the model *Ctrl* run (0.26 m s^{-1} $°C^{-1}$) compared to the observed (0.35 m s^{-1} $°C^{-1}$). It is also worth noting that the underestimation of the coupling coefficient has already been documented in several papers (Renault *et al*., 2016a; 2016b; Oerder *et al*., 2015). Perlin *et al*. (2007) also noticed an underestimation of the coupling coefficient in the Agulhas retroflection current by using the MYNN2 PBL scheme. The same analysis performed over the BUS and the ABFZ (not shown), suggests that the thermal control of the stability of the atmospheric surface layer also occurs over these oceanic mesoscale patterns.

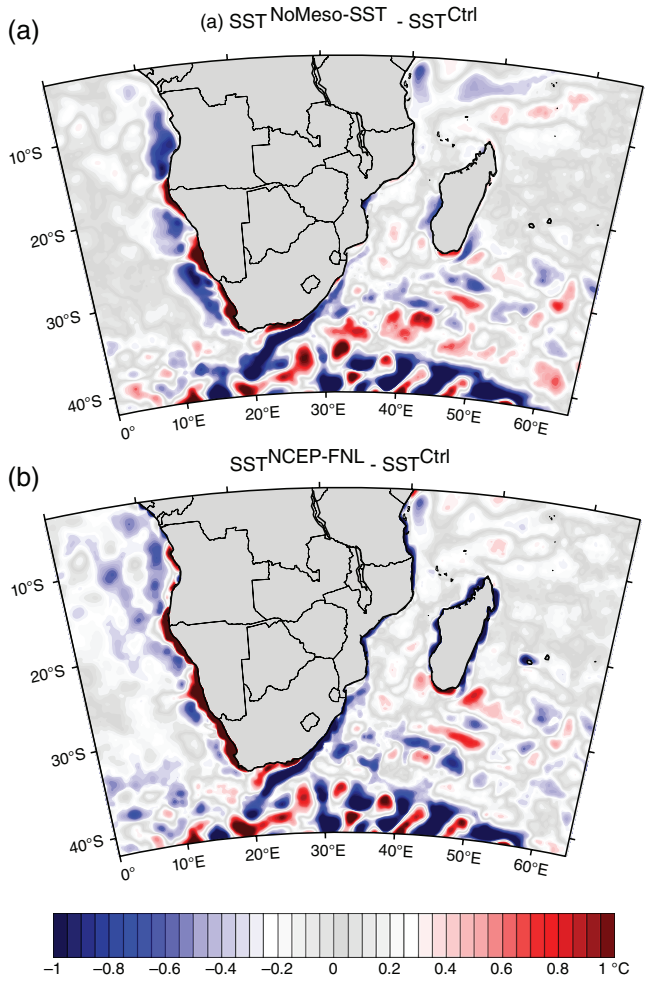

FIGURE 2 Mean biases between (a) the two SST forcings used and (b) NCEP-FNL SST and OSTIA SST, averaged over the 2008–2009 austral summer (DJF). Data are interpolated onto the WRF grid and the unit is °C [Colour figure can be viewed at wileyonlinelibrary.com]

The spatial variance of the oceanic 10 m surface wind speed is drastically impacted when removing the SST mesoscale activity. The surface wind speed spatial variance, a good proxy for the presence of fine-scale variations, is significantly larger in the *Ctrl* runs compared to *noMeso-SST*. For instance, over the Agulhas (black box in Figure 1a), the 10 m wind spatial variance averaged during austral summer is 0.78 m^2/s^2 for *Ctrl* run and 0.47 m^2/s^2 for *noMeso-SST* run. This result is consistent with ECMWF outputs analyses when SST forcing is changed (Song *et al*., 2009). According to these authors, SST mesoscale variations significantly increase the fine-scale variability of the wind for spatial scales up to 1,000 km.

Lastly, and to support the methodology used, Figure 2a, b shows the summer-mean difference between the *noMeso-SST* and the *Ctrl* SST forcing and the NCEP-FNL SST and the *Ctrl* SST (i.e., OSTIA), respectively. Although the spatial average of the two SST forcings is essentially the same (<0.03 °C over the summer period), there are large differences in some regions, particularly along the west coast of southern Africa in the BUS as well as north of the ABFZ, and in the Agulhas Current, its retroflection and the Agulhas Return Current in the South Indian Ocean (Figure 2a). The filtering process used to create *noMeso-SST* has removed not only the intermittent features associated with ocean eddies but has also created some permanent biases. Nevertheless, it is important to note that the mean bias generated by the filtering method corresponds to biases found in coarse resolution SST data sets such as NCEP-FNL (Figure 2b). Hereafter, the differences interpreted between the two ensemble-mean simulations (*Ctrl* and *noMeso-SST*) can be

attributed to the effective resolution of the SST used to force WRF model. The effective resolution of the different SST products frequently used to force an atmospheric model is discussed in section 5.

3 | RESPONSE OF ATMOSPHERIC PROFILES TO MESOSCALE SST PATTERNS AND CONSEQUENCES FOR INCOMING MOISTURE FLUXES

In this section, we address the air-column responses above SST anomalies between the two runs, which correspond to mesoscale patterns introduced in *Ctrl.* Anomalies are defined as the difference between *noMeso-SST* and the *Ctrl* runs. SST anomalies larger (smaller) than (−)1 °C have been tracked in space and time to construct the response of the composite state of the air-column. We first consider SST anomalies within the Agulhas region (black box in Figure 1a) which typically exhibits strong anomalies between the two forcing fields (see Figure 2a). Figure 3 displays composite atmospheric vertical anomaly profiles of temperature, horizontal wind amplitude, specific humidity, and vertical wind, above anomalous warm (Figure 3a) and cold (Figure 3b) SST anomaly structures. Over warm anomalies (~60,000 vertical profiles), the *Ctrl* run is warmer, with more humidity, upward motion, and horizontal wind from the sea surface up to ~2 km height (Figure 3a). Both air temperature and horizontal wind speed anomalies show a sign inversion at ~2 km but become again positive at ~4 km above the sea level. The convection (positive upward wind anomaly) is favoured up to 4 km above the sea level. Humidity anomalies are significantly positive until ~5,000 m. Over cold SST anomalies (~80,000 vertical profiles), the vertical response of the atmosphere is stronger (Figure 3b). This is especially true for the horizontal wind speed which shows negative values up to 13 km height above negative SST anomalies. Although temperature and humidity anomalies change sign, vertical wind anomalies are negative (favouring subsidence) up to 10 km above the sea surface. Humidity anomalies within the PBL (~2 km in both sets of experiments) remain negative over cold SST structures. Because the humidity difference comes from the SST applied at the surface, anomalies in air-column humidity appear to be a good proxy to evaluate the maximum height at which the ocean thermodynamics impact the atmospheric column. In both cases, this altitude is ~5 km (Figure 3a,b) which is higher than the PBL height. This result shows that the mesoscale thermal coupling between SST and MABL dynamics which acts in the lower atmosphere layer and can also modify the properties of the troposphere.

Given the influence of mesoscale SST structures on the wind, the moisture flux is also affected, and the water vapour content in the lower troposphere is strongly modified between the two simulations, through transport and mixing processes. Figure 3c shows the austral summer-mean (DJF) vertically integrated moisture flux for both simulations and the vapour content anomaly. The vertical integration is performed over the lowest 5 km of the atmosphere, which corresponds to the altitude where vapour content anomalies become non-significant (Figure 3a,b). A positive anomaly means more vapour content in the *NoMeso-SST* runs. The moisture flux entering the southern African continent during austral summer occurs through three key regions (namely tropical western Indian Ocean, southwest Indian Ocean, and tropical southeast Atlantic Ocean; Reason *et al*., 2006), schematically represented in red in Figure 3c. Results show that mesoscale variations of SST tend to decrease the incoming moisture flux onto the continent from the tropical regions, especially for that from the tropical Indian Ocean (a reduction of approximately 25%; see Figure 3c). The maroon lines in Figure 4a,b (discussed further in section 4) show that the Intertropical Convergence Zone (ITCZ; characterized by strong surface wind convergence and convective activity and associated rainfall) lies further north in the *NoMeso-SST* run especially over Madagascar and it is oriented more zonally through the northern part of the Mozambique Channel. Hence, the mesoscale SST forcing leads to substantial differences in the ITCZ position and in the source of incoming flux through this section. The incoming moisture flux is slightly reduced in the *Ctrl* run in the tropical Atlantic (−12%; Figure 3c). These differences imply higher water vapour content (positive vertically integrated humidity anomalies) within the lower atmosphere in the *NoMeso-SST* run in the tropical part of the domain. It is worth noting that the heat content between the two prescribed SST forcings is not modified (as shown by the absence of SST contours in the tropical part of oceanic domain; Figure 3c). Therefore, the local effect of the SST-MABL stability interactions seems to play an important role at a larger scale and the remote effects are important. Through the southwest Indian Ocean section (i.e., Mozambique Channel), the moisture flux is promoted by the mesoscale SST variability (+7%), and the vertically integrated humidity, larger in the *Ctrl* run, flows across the continent and supplies water vapour to both Botswana and central southern Africa. More generally, the differences in moisture flux can be explained either by wind or humidity anomalies or both. In the lowest layer of the MABL, water vapour content anomalies correspond to SST anomalies (not shown). Over the continent, more (less) water vapour content is generally evident in the *Ctrl* run in the southern (northern) part of the domain (Figure 3c). This is especially true over the Botswana and southern Zimbabwe regions.

4 | UPSCALING EFFECTS

In this section, we consider the austral summer mean atmospheric circulation over southern Africa. Figure 4a,b

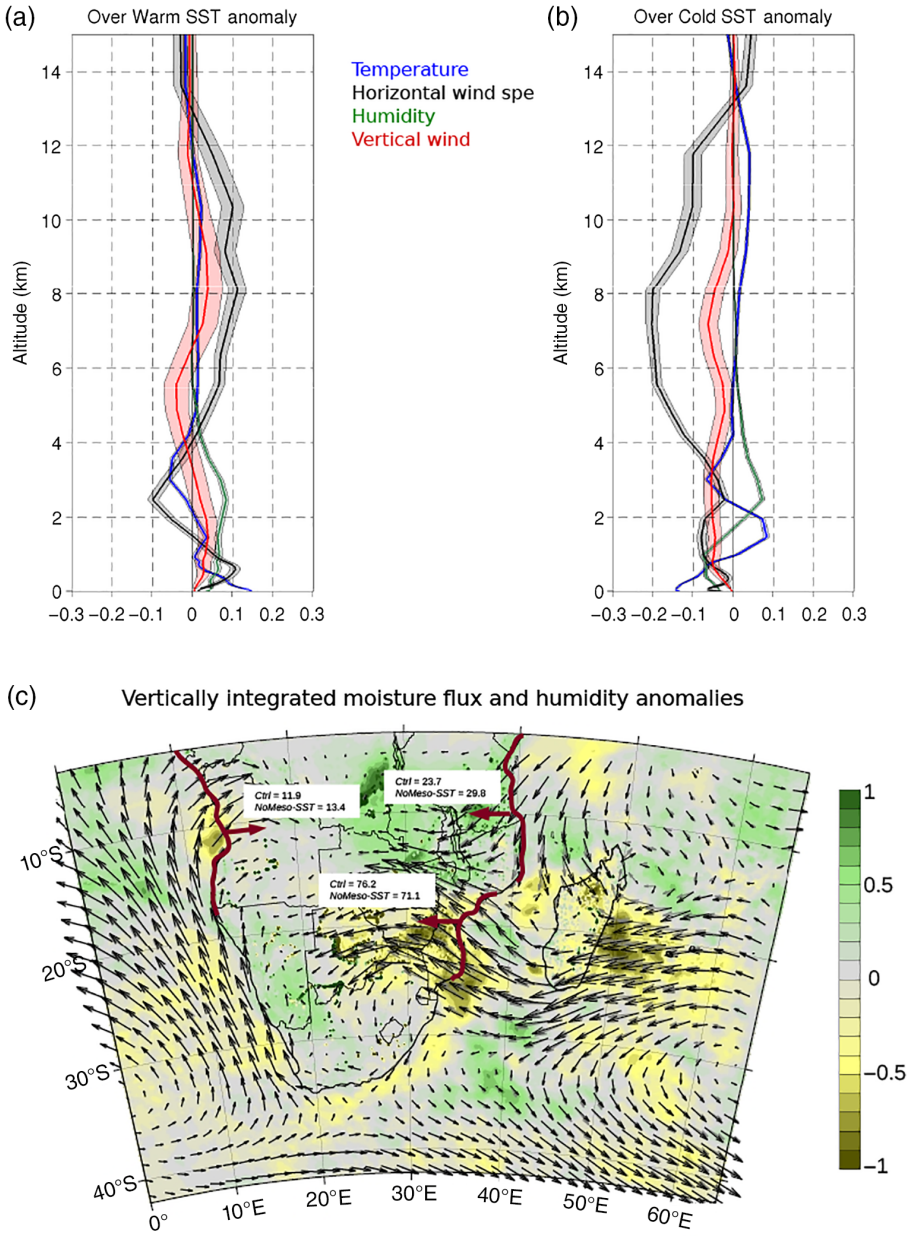

FIGURE 3 Composite vertical anomaly profiles (*noMeso-SST* minus *Ctrl*) of air temperature (blue), horizontal wind (black, m/s), specific humidity (green, 10^{-4} kg/m^2) and upward wind (red, 10^{-3} m/s) over anomalous warm (a) and cold (b) structures. Shaded area represent $\pm SD$ obtained using a bootstrap method. (c) Austral summer (DJF) average of vertically integrated vapour content anomalies (colours, g/kg) and moisture flux (black and grey arrow for *Ctrl* and *noMeso-SST*, respectively, in g kg^{-1} s^{-1}) from surface to 5 km height [Colour figure can be viewed at wileyonlinelibrary.com]

shows DJF surface wind speed and direction (arrows) and geopotential height at 800 hPa (contours) for *Ctrl* and *noMeso-SST* runs, respectively. The position of the ITCZ (maroon dashed lines) is determined from the maximum wind convergence at 10 m height. Figure 4c–e displays the seasonal mean differences between the two simulations (*noMeso-SST* minus *Crtl*) in terms of daily rainfall, the top-of-atmosphere (TOA) radiation, and air temperature at 2 m during the austral summer, respectively.

The main differences between the two simulations in surface wind speed are located over the coastal areas of the BUS, the Mozambique Chanel, and over the Agulhas retroflection zone (not shown). This result is consistent since these areas are characterized by strong oceanic mesoscale activity. Taking into account the mesoscale dynamics of ocean surface plays an essential role in shaping the southern boundary of the ITCZ. This is especially true over Madagascar and the Mozambique Channel where mesoscale variations of SST favour a southern shift of the ITCZ, with an NW-SE orientation. The pattern in rainfall differences is then accentuated over this area (Figure 4c) due to convection associated with moisture convergence. Notably, a strong anomalous dipole in the rainfall exists, and the *NoMeso-SST* run is drier over the Mozambique Channel associated with the ITCZ location (Figure 4a,b, see also the vertically integrated humidity anomalies in Figure 3a,b). More interestingly, the *Ctrl* experiments also show higher summer rainfall from the Mozambique coast extending inland to Botswana.

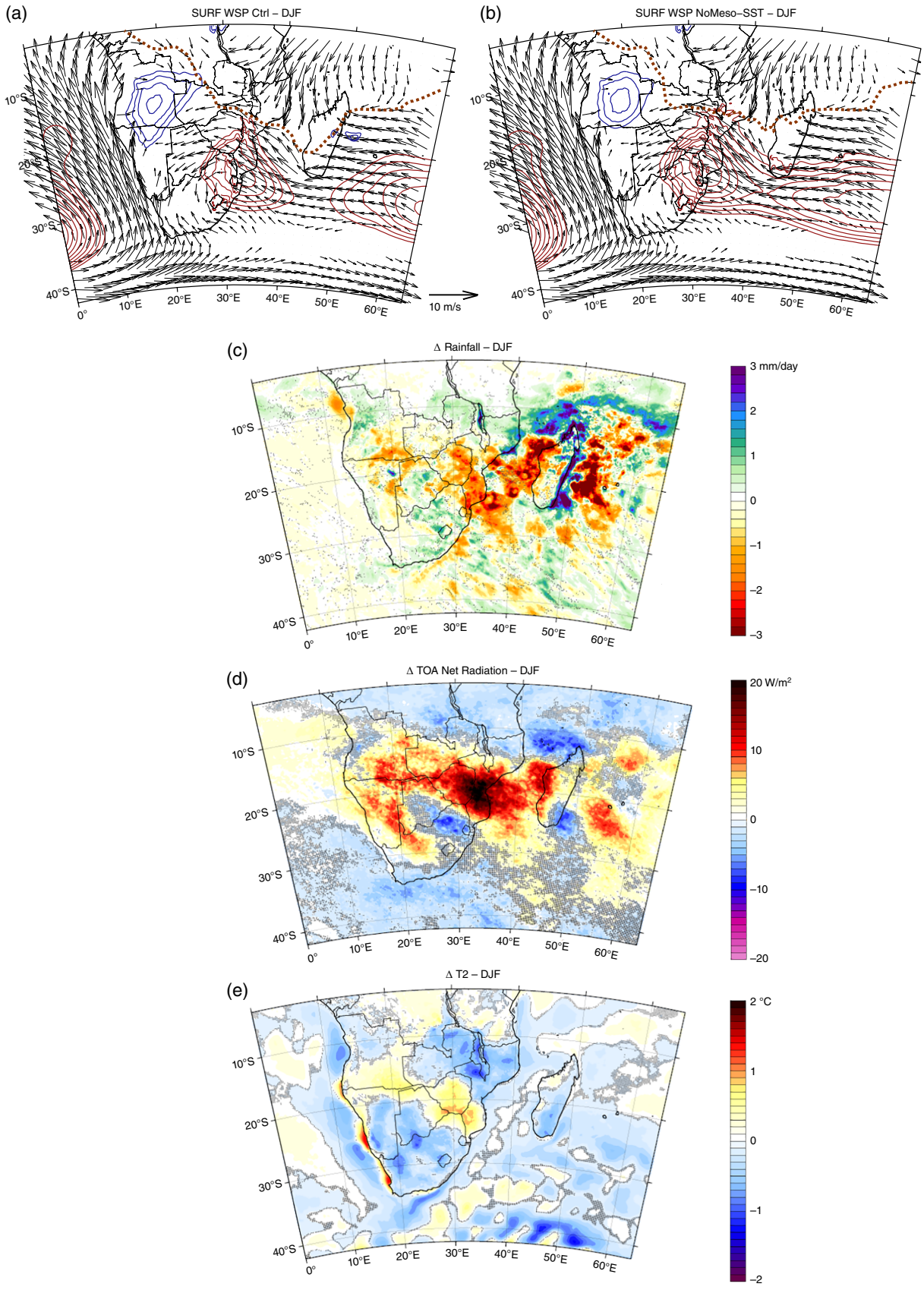

FIGURE 4 (a, b) Surface wind speed (m/s) and direction (coloured arrows) and geopotential height at 800 hPa (in m, red and blue contours) for *Crtl* and *noMeso-SST* runs, respectively. The maroon line represents the southern boundary of the ITCZ. (c) Mean of daily rainfall anomaly (mm/day). (d) Anomaly of top-of-atmosphere radiation (W/m^2) and (e) 2 m air temperature (°C). Anomalies are *noMeso-SST* minus *Ctrl* outputs. Fields are averaged during austral summer (DJF). (c–e) Only anomalies for which the Wilcoxon signed rank test *p*-value (Wilcoxon, 1945) are larger than .05 are displayed, the remaining areas are shown in hatching. This statistical test is adapted for small, non-normally distributed samples [Colour figure can be viewed at wileyonlinelibrary.com]

Relatively large differences in geopotential height at 800 hPa (see contour lines in Figure 4a,b) occur around both subtropical high-pressure cells in the South Indian and South Atlantic Oceans and in the Angola Low. Anticyclonic winds associated with the high-pressure cells are more intense in the *Ctrl* runs, especially for the pressure cells in the east of the domain (the South Indian Ocean High and the Botswana High; see Figure 4a,b; Reason, 2016; Driver and Reason, 2017). The Angola Low is stronger in the *Ctrl* runs with stronger pressure gradients between it and the neighbouring regions. This system strongly influences the austral summer rainfall over southern Africa notably through the creation of cloudbands (Mulenga *et al*., 2003; Cook *et al*., 2004; Hart *et al*., 2013; Munday and Washington, 2017). Because these cloudbands are oriented to the southeast from the Angola Low, increased rainfall over Botswana and central/southern Africa results. The TOA radiation shows positive/negative differences consistent with the rainfall differences and cloudband activity over eastern Botswana and Zimbabwe. The imprint of a more-pronounced gradient in the Agulhas Current seems also important in terms of rainfall (Figure 4c) as well as vertically integrated humidity (Figure 3c), with important negative differences in rainfall observed along the eastern coast of South Africa. The austral summer rainfall differences over the continent are consistent with the vapour content anomalies (Figure 3c; section 3).

Lastly, the austral summer-mean 2 m air temperature shows a positive difference over the drier coastal fringe of western South Africa and Namibia and a negative difference inland. In the stronger Angola Low region, despite it favouring increased cloud cover, the 2 m air temperature difference is slightly positive. This result also highlights the importance of the SST variability in the BUS. As an example, the main upwelling cells (characterized in our case as important SST bias between the two forcings, see Figure 2a) are identified in important 2 m air temperature difference and minor cloud cover differences (Figure 4e,d). An important SST bias favours cloud formations in the warmer boundary condition (*NoMeso-SST*), but these clouds may not be important for rainfall production because no obvious differences are noticed in Figure 4c. As a general rule, a well-defined upwelling front acts to reduce the surface air temperature over the adjacent coastal area by up to 1 °C (Figure 4e). The mesoscale SST variability in *Ctrl* runs also leads to cooler (warmer) air temperature north (south) of the ABFZ and reduced rainfall over coastal Angola. Finally, as expected, a strong correspondence is noticed between SST and 2 m air temperature differences, notably over Agulhas Current and its retroflection and over the main upwelling cells (Figure 4e).

5 | CONCLUDING REMARKS

The integrated imprint of mesoscale SST variability on the atmospheric austral summer circulation over southern Africa has been examined through sensitivity experiments using the WRF model. The modifications of local surface winds are notable over major ocean fronts and regions with strong SST gradients and mesoscale activity (i.e., Agulhas rings and retroflection, BUS, and ABFZ). The atmospheric column above these mesoscale structures is also strongly modified. For example, the air-column properties are modified above the MABL. A slight difference is noticed in atmospheric profile response between cold and warm SST anomalies. The transition from unstable to stable air-column (cool to warm SST) seems to favour a more obvious response in the overlying atmospheric column. This result highlights the coupling between MABL processes and atmospheric processes aloft. However, this result seems restricted to the open ocean since the air-column responses of mesoscale SST variations are confined within the MABL in coastal areas. This is especially the case for the Benguela Jet (along South Africa/Namibia coast). In contrast with the dynamics above the open ocean, the atmosphere here is constrained by the coast, and its characteristics (Patricola and Chang, 2017), which results in a decoupling of the MABL response to upper atmospheric layer.

Because of nonlinear dynamics, the upscaling effects of the thermodynamical link between SST variability and MABL dynamics are important at regional and seasonal scales. The mesoscale SST variability leads to changes in the mean position of the ITCZ in the Indian Ocean part of the domain. The processes associated with wind convergence are then modified leading to substantial differences in austral summer rainfall and moisture flux entering southern Africa. The Angola Low pressure system, an important feature for tropical–extra-tropical interactions and the development of cloudbands (a key local rainfall producer) over southern Africa is more intense with the presence of mesoscale activity. However, this study only considered one specific summer (2008–2009) which correspond to a neutral ENSO year. It is important to note that ENSO strongly influences regional circulation and rainfall over southern Africa (Lindesay, 1988; Reason *et al*., 2000). Nonetheless, the results do suggest the essential role of high resolution SST forcing in air–sea interaction processes and hence in regional climate simulations.

In this regard, Figure 5 displays the spatial power spectra of SST data commonly used by the atmospheric model community. OSTIA SST, used in this study, appears to be one of the better options in term of effective scales, along with the multi-scale ultra-high resolution (MUR) SST. Commonly available reanalysis data (e.g., NCEP-FNL, CFSR, and ERA-Interim) do not contain sufficient details when taking into account SST–wind interactions, which can lead to important seasonal biases for long-term simulations. The power spectra of these reanalysis SST data set are equivalent to the one calculated with the smoothed-OSTIA data used in *NoMeso-SST* experiments. Therefore, we suggest that there

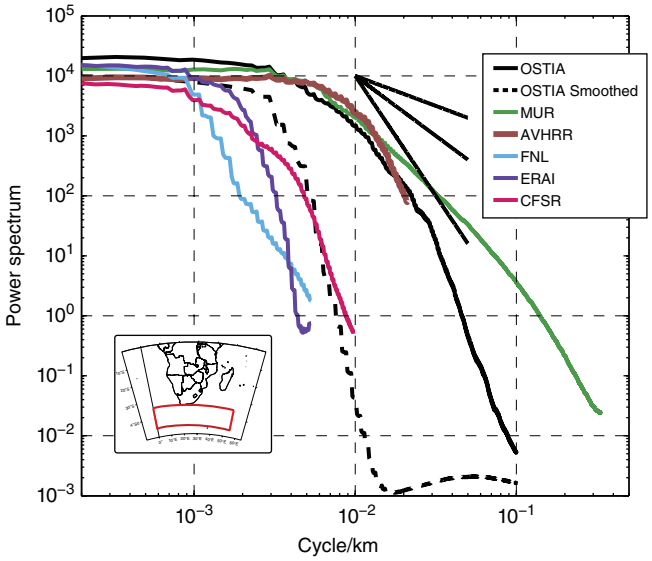

FIGURE 5 One-month (January 2009) average of daily wave number spectra ($°C^2$) of commonly used SST fields: OSTIA (black line), OSTIA-smoothed (black dashed line), MUR (green line), AVHRR (brown line), FNL (blue line), ERA-INTERIM (purple line) and CFSR (pink line) SST. The theoretical profiles in k^{-1} and k^{-2}, and k^{-4} are drawn for the comparison. Spectra are computed using SST data interpolated onto the MUR grid (highest resolution) and over the domain framed in the map insert in the bottom left corner [Colour figure can be viewed at wileyonlinelibrary.com]

may be substantial summer-mean biases in the regional circulation and rainfall in models forced by these data. Other satellite products commonly used to describe variability, to study air-sea interactions and as a forcing field for atmospheric models are also shown as examples (AVHRR; Casey *et al*., 2010).

Although this study has highlighted the influence of coupled ocean–atmosphere interactions around southern Africa, there are still many gaps in the knowledge regarding the influence of specific ocean domains on the neighbouring African continent. In order to disentangle the various coupling processes and feedbacks, ongoing process-based studies, such as quantifying the role of ABZF variability on the Angola Low system, are currently underway. The importance of such studies is that they not only assist in improving our understanding of the influence of the ocean on the regional climate, but also contribute to the scientific community through the identification of the strengths and limitations of the various data sets and methods that are currently used in climate research.

ACKNOWLEDGEMENTS

This research was supported by NERC (Natural Environment Research Council), as part of the UMFULA project funded by the FCFA (Future Climate For Africa) program. F.D., R.B., R.J., R.B., and C.J.C.R. are directly linked to the project. Support for this study has also been provided by UCT for F.D., R.B., R.J., R.B., and C.J.C.R., IRD (Institut de Recherche et de Developement) for S.I. and L.R., by the National Research Foundation (NRF) for L.R. Authors thanks Dr. Aude Illig for fruitful discussions on statistics. All data used in this study are freely available by the following ftp or url, namely, OSTIA SST (ftp://podaac-ftp.jpl.nasa.gov/ allData/ghrsst/data/L4/GLOB/UKMO/OSTIA/), MUR SST (https://podaac.jpl.nasa.gov/dataset/JPL-L4UHfnd-GLOB-MUR), AVHRR SST (ftp://eclipse.ncdc.noaa.gov/pub/OI-daily-v2/NetCDF/), and QuikSCAT L3 data (ftp://ftp.ifremer.fr/ifremer/cersat/products/gridded/MWF/L3/QuikSCAT/Daily/Netcdf/). The model configurations have been developed using facilities provided by ICTS High Performance Computing team at UCT (http://hpc.uct.ac.za) and the CSAG computing facility CORE. The ensemble-simulations have been run on the national UK Cluster ARCHER.

ORCID

Fabien Desbiolles http://orcid.org/0000-0002-8047-602X
Ross Blamey http://orcid.org/0000-0001-7941-326X
Chris Reason http://orcid.org/0000-0002-3224-5243

REFERENCES

Behera, S.K. and Yamagata, T. (2001) Subtropical SST dipole events in the southern Indian Ocean. *Geophysical Research Letters*, 28, 327–330.

Casey, K.S., Brandon, T.B., Cornillon, P. and Evans, R. (2010) The past, present, and future of the AVHRR pathfinder SST program. In: *Oceanography from Space*. Dordrecht: Springer, pp. 273–287.

Chang, P. and Philander, S.G. (1994) A coupled ocean–atmosphere instability of relevance to the seasonal cycle. *Journal of the Atmospheric Sciences*, 51(24), 3627–3648.

Chelton, D.B. and Xie, S.P. (2010). Coupled ocean–atmosphere interaction at oceanic mesoscales. *Oceanography*, 23(4), 52–69.

Chelton, D.B., Schlax, M.G., Freilich, M.H. and Milliff, R.F. (2004) Satellite measurements reveal persistent small-scale features in ocean winds. *Science*, 303, 978–983.

Chelton, D.B., Schlax, M.G. and Samelson, R.M. (2007) Summertime coupling between sea surface temperature and wind stress in the California Current System. *Journal of Physical Oceanography*, 37(3), 495–517.

Cook, C., Reason, C.J.C. and Hewitson, B.C. (2004) Wet and dry spells within particularly wet and dry summers in the South African summer rainfall region. *Climate Research*, 26, 17–31.

Dee, D.P., Uppala, S.M., Simmons, A.J., Berrisford, P., Poli, P., Kobayashi, S., Andrae, U., Balmaseda, M.A., Balsamo, G., Bauer, D.P. and Bechtold, P. (2011) The ERA-Interim reanalysis: Configuration and performance of the data assimilation system. *Quarterly Journal of the royal meteorological society*, 137(656), 553–597.

Desbiolles, F., Blanke, B., Bentamy, A. and Grima, N. (2014) Origin of fine-scale wind stress curl structures in the Benguela and canary upwelling systems. *Journal of Geophysical Research: Oceans*, 119(11), 7931–7948.

Desbiolles, F., Bentamy, A., Blanke, B., Roy, C., Mestas-Nunez Alberto, M., Grodsky Semyon, A., Herbette, S., Cambon, G. and Maes, C. (2017) Two decades [1992–2012] of surface wind analyses based on satellite scatterometer observations. *Journal of Marine Systems*, 168, 38–56.

Driver, P. and Reason, C.J.C. (2017) Variability in the Botswana high and its relationships with rainfall and temperature characteristics over southern Africa. *International Journal of Climatology*, 37(S1), 570–581.

Gill, A.E. (1982) *Atmosphere–Ocean Dynamics*. San Diego: Academic Press, 662 pp.

Hart, N.C., Reason, C.J. and Fauchereau, N. (2013) Cloud bands over southern Africa: seasonality, contribution to rainfall variability and modulation by the MJO. *Climate Dynamics*, 41(5–6), 1199–1212.

Lefèvre, J., Marchesiello, P., Jourdain, N.C., Menkes, C. and Leroy, A. (2010) Weather regimes and orographic circulation around New Caledonia. *Marine Pollution Bulletin*, 61(7), 413–431.

Lindesay, J.A. (1988) South African rainfall, the Southern Oscillation and a Southern Hemisphere semi-annual cycle. *Journal of Climatology*, 8(1), 17–30.

Mason, S. (1995) Sea-surface temperature–South African rainfall associations, 1910–1989. *International Journal of Climatology*, 15, 119–135.

Milliff, R.F., Morzel, J., Chelton, D.B. and Freilich, M.H. (2004) Wind stress curl and wind stress divergence biases from rain effects on QSCAT surface wind retrievals. *Journal of Atmospheric and Oceanic Technology*, 21(8), 1216–1231.

Minobe, S., Kuwano-Yoshida, A., Komori, N., Xie, S.P. and Small, R.J. (2008) Influence of the Gulf Stream on the troposphere. *Nature*, 452(7184), 206–209.

Mulenga, H.M., Rouault, M. and Reason, C.J.C. (2003) Dry summers over northeastern South Africa and associated circulation anomalies. *Climate Research*, 25(1), 29–41.

Munday, C. and Washington, R. (2017) Circulation controls on southern African precipitation in coupled models: the role of the Angola Low. *Journal of Geophysical Research: Atmospheres*, 122(2), 861–877.

O'Neill, L.W., Chelton, D.B. and Esbensen, S.K. (2010) The effects of SST-induced surface wind speed and direction gradients on midlatitude surface vorticity and divergence. *Journal of Climate*, 23, 255–281.

Oerder, V., Colas, F., Echevin, V., Codron, F., Tam, J. and Belmadani, A. (2015) Peru–Chile upwelling dynamics under climate change. *Journal of Geophysical Research: Oceans*, 120(2), 1152–1172.

Patricola, C.M. and Chang, P. (2017) Structure and dynamics of the Benguela low-level coastal jet. *Climate Dynamics*, 49(7–8), 2765–2788.

Perlin, N., Skyllingstad, E.D., Samelson, R.M. and Barbour, P.L. (2007) Numerical simulation of air–sea coupling during coastal upwelling. *Journal of Physical Oceanography*, 37(8), 2081–2093.

Reason, C.J.C. (2016) The Bolivian, Botswana, and Bilybara Highs and Southern Hemisphere drought/floods. *Geophysical Research Letters*, 43(3), 1280–1286.

Reason, C.J.C. and Mulenga, H.M. (1999) Relationship between South African rainfall and SST anomalies in the southwest Indian Ocean. *International Journal of Climatology*, 19, 1652–1673.

Reason, C.J.C., Allan, R.J., Lindesay, J.A. and Ansell, T.J. (2000) ENSO and climatic signals across the Indian Ocean basin in the global context: part I, interannual composite patterns. *International Journal of Climatology*, 20, 1285–1327.

Reason, C.J.C., Landman, W. and Tennant, W. (2006) Seasonal to decadal prediction of southern African climate and its links with variability of the Atlantic Ocean. *Bulletin of the American Meteorological Society*, 87, 941–955.

Renault, L., Hall, A. and McWilliams, J.C. (2016a) Orographic shaping of US West Coast wind profiles during the upwelling season. *Climate Dynamics*, 46(1–2), 273–289.

Renault, L., Molemaker, M.J., McWilliams, J.C., Shchepetkin, A.F., Lemarié, F., Chelton, D., Illig, S. and Hall, A. (2016b) Modulation of wind work by oceanic current interaction with the atmosphere. *Journal of Physical Oceanography*, 46(6), 1685–1704.

Saha, S., Moorthi, S., Wu, X., Wang, J., Nadiga, S., Tripp, P., Behringer, D., Hou, Y.T., Chuang, H.Y., Iredell, M. and Ek, M. (2014) The NCEP climate forecast system version 2. *Journal of Climate*, 27(6), 2185–2208.

Skamarock, W.C., Klemp, J.B., Dudhia, J., Gill, D.O., Barker, D.M., Wang, W. and Powers, J.G. (2005) *A description of the advanced research WRF version 2*. Boulder, CO: National Center for Atmospheric Research. NCAR technical note NCAR/TN-468+STR.

Small, R.J., deSzoeke, S.P., Xie, S.P., O'Neill, L., Seo, H., Song, Q., Cornillon, P., Spall, M. and Minobe, S. (2008) Air–sea interaction over ocean fronts and eddies. *Dynamics of Atmospheres and Oceans*, 45, 274–319.

Song, Q., Chelton, D.B., Esbensen, S.K., Thum, N. and O'Neill, L.W. (2009) Coupling between sea surface temperature and low-level winds in mesoscale numerical models. *Journal of Climate*, 22(1), 146–164.

Stark, J.D., Donlon, C.J., Martin, M.J. and McCulloch, M.E. (2007) OSTIA: an operational, high resolution, real time, global sea surface temperature analysis system. In: *Oceans 2007—Europe*. Victoria, Canada: IEEE, pp. 1–4.

Wilcoxon, F. (1945) Individual comparisons by ranking methods. *Biometrics Bulletin*, 1, 80–83. https://doi.org/10.2307/3001968.

How to cite this article: Desbiolles F, Blamey R, Illig S, *et al.* Upscaling impact of wind/sea surface temperature mesoscale interactions on southern Africa austral summer climate. *Int J Climatol*. 2018;38: 4651–4660. https://doi.org/10.1002/joc.5726